HELIOS - Highly rEliable Links durIng sOlar conjunctionS

A. Zeqaj[1*], P. Tortora[1], E. Paolini[2], A.J. Stocker[3], D.R. Siddle[3], A. Argyriou[4], J. De Vicente[5], R. Abello[5†], M. Mercolino[5]

[1]Department of Industrial Engineering, University of Bologna, Forlì, Italy
[2]Department of Electrical, Electronic and Information Engineering, University of Bologna, Cesena, Italy
[3]Department of Engineering, University of Leicester, Leicester, UK
[4]Department of Electrical & Computer Engineering, University of Thessaly, Volos, Greece
[5]European Space Operations Center, European Space Agency, Darmstadt, Germany

Key Points:

- Solar Conjunctions
- PLL
- Non-coherent Modulation
- TT&C
- LDPC

* Currently at Deutsches Zentrum für Luft- und Raumfahrt e.V. (DLR)
† Retired

Corresponding author: Aurel Zeqaj, aurel.zeqaj2@unibo.it

Abstract

During deep space missions, maintaining reliable communication between a spacecraft and Earth becomes particularly challenging during superior solar conjunctions, when the spacecraft passes behind the Sun relative to Earth. The highly ionized solar corona and solar wind create plasma inhomogeneities that severely affect radio signals, leading to phase scintillation, amplitude fading, and signal loss. These effects intensify as the Sun-Earth-Probe (SEP) angle decreases, resulting in frequent disruption of phase-locking techniques crucial for telecommunication.

This paper comprehensively analyzes a communication subsystem architecture designed to ensure reliable tracking, telemetry, and command (TT&C) links during superior solar conjunctions. By analyzing the effects of solar plasma on radio links, the paper proposes new operational methods and subsystem architectures that enhance the robustness of RF communication even in the harshest conditions. The solutions include optimized modulation, coding schemes, non-coherent modulation methods, and alternative channel models to mitigate scintillation effects and maintain stable communication links, particularly at low SEP angles. These strategies offer promising ways to improve data transmission reliability and maximize mission success during challenging solar conjunction phases.

Plain Language Summary

During a deep space mission, there are times when the spacecraft lies behind the Sun, as seen from the Earth. When these events (called superior solar conjunctions) occur, the charged plasma ejected by the Sun in the so-called solar wind corrupts the telecommunication signals up to a point that can make it impossible to receive data or send commands to the spacecraft, for periods that can last hours to months, depending on the relative geometries. In this paper, we propose some alternative/new technologies that can help mitigate this phenomenon.

1 Introduction

Maintaining communication with a spacecraft during superior solar conjunctions presents significant challenges due to the Sun's corona, i.e. a region of highly ionized plasma that distorts radio signals (Li et al., 2012; D. D. Morabito, 2007; D. Morabito et al., 2003). When the propagation path between the Earth and a distant spacecraft lies close to the Sun, as it does during superior solar conjunctions, the coronal plasma can have severe effects on the communications channel through, for example, the introduction of amplitude and phase scintillations (Woo, Yang, & Ishimaru, 1976; Woo, Yang, Yip, & Kendall, 1976; Pätzold et al., 2012; Verma et al., 2013).

Due to the presence of plasma blobs (i.e. inhomogeneities in the electron density of the solar wind), which move across the carrier wave path, there is an increased degradation in terms of amplitude and phase scintillation, as well as spectral broadening (Figure 1). These effects scale with the electron content of the medium that is being crossed by an RF signal and with the signal frequency: in particular, scintillation is less severe at higher carrier frequencies (Feria et al., 1997; Bertotti et al., 1993; Mariotti & Tortora, 2013). As might be expected, as the path between the spacecraft and the Earth gets closer to the Sun (i.e., as the SEP angle gets smaller), the effect of the solar plasma on the signal tends to increase. For space radio links with a Line-of-Sight (LoS) that crosses the corona, the effect depends upon the electron density of the coronal layer that is encountered (with a higher density in the regions closer to the sun), while outside the corona the effect of solar plasma on the signal depends on the solar wind velocity component normal to the LoS vector (Tortora et al., 2002; Ho, 2005; Armstrong et al., 1979).

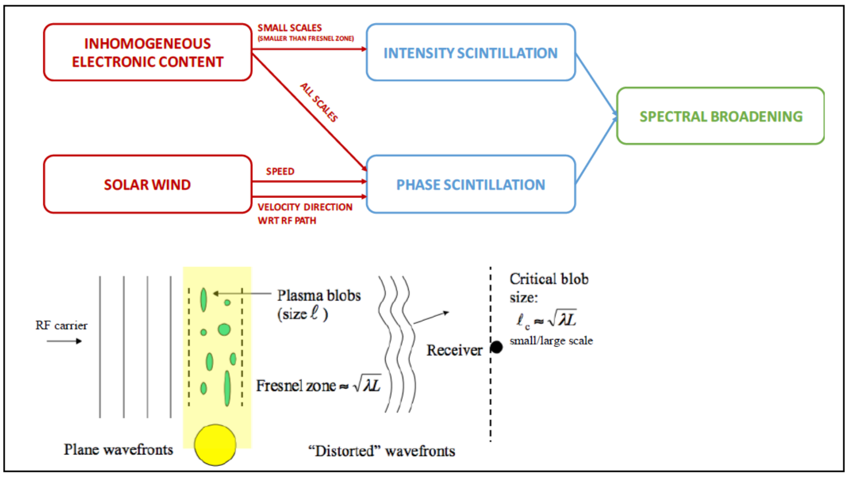

Figure 1. Solar plasma effects on RF signals.

Various statistical models, including the Rician fading model (Feria et al., 1997; D. Morabito et al., 2003; D. D. Morabito, 2007), have been used to describe the probability distribution of amplitude and phase scintillations. While the amplitude scintillation behavior is known for very low SEP angles (e.g., (Lanucara, 2013)), the phase scintillation model reported by (Kinman, 2003), which is based on measurements reported by (Woo & Armstrong, 1979), is limited to SEP angles greater than 5°. Furthermore, while the performance of several communication systems (e.g., different modulation types, radio frequencies, etc.) have been calculated based on analytic or semi-analytic solutions of the amplitude and phase scintillation effects, only a few complete system performance simulators have been used (e.g., (Feria et al., 1997)), mainly because to do so is "time-consuming and not practical at the lower Bit Error Rates (BER) of interest." Recent improvements in computing resources have made this approach more practicable.

Maintaining reliable communication links during superior solar conjunctions is a challenging problem for all these reasons. In some cases, existing modulation and coding schemes have proven effective in improving Bit Error Rate (BER) and Frame Error Rate (FER), but they fall short in most extreme conditions. As SEP angles approach zero, combining high plasma density and signal distortions renders traditional techniques ineffective. This highlights the need for more innovative approaches to ensure communication stability during these critical periods (Finocchiaro et al., 2017).

The HELIOS project succeeded in defining a communication subsystem architecture (including ground and space segments, as well as operational methods) that allows robust RF TT&C links during superior solar conjunction phases. The defined architectures ensure reliable links, at the cost of reducing data volumes, and also at high scintillation regimes (i.e., very low SEP angles, where scintillations still dominate over thermal noise effects).

2 Channel Model

As part of the Helios project, (A. J. Stocker et al., 2018; A. Stocker et al., 2017) introduced a comprehensive channel model for X-band signals propagating through the solar corona. This model has been derived based on experimentally determined Power Spectral Densities (PSDs) of signal amplitude and phase variations (reflecting the fluctuations observed during actual space missions, such as those recorded from Mars Express (MEX) during its 2013 solar conjunction). Notably, the phase model developed ex-

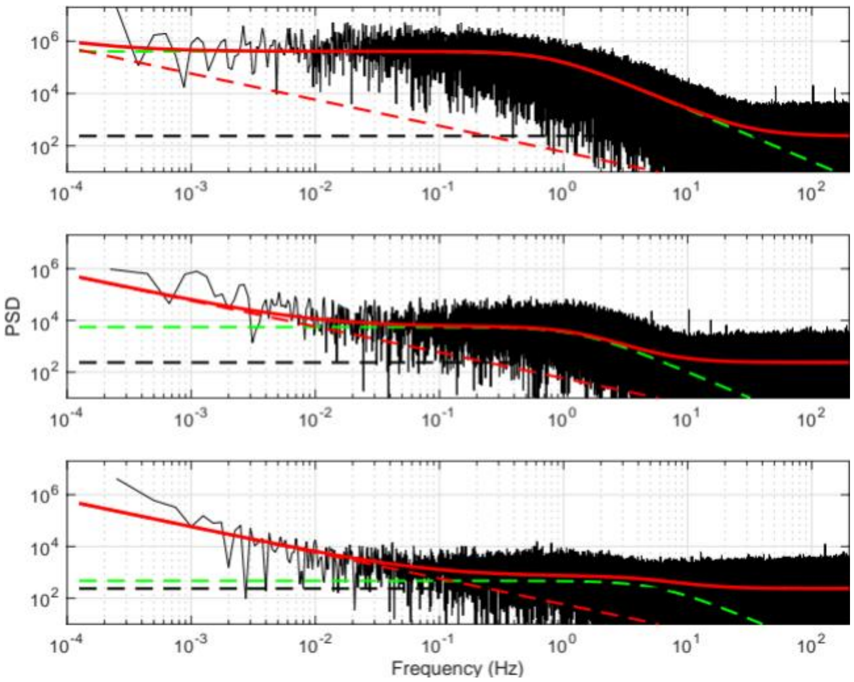

Figure 2. PSD spectrum of amplitude scintillation for (from the top) SEP=2.4°, 5.6°, and 9.0°. The best-fit curves of the overall PSD (solid red line), the white noise floor (dashed black line), solar effects (dashed green line), and pink noise (dashed red line) are also indicated.

tends the range of SEP angles that can be accurately modeled from 5° to approximately 0.8°, providing enhanced modeling capabilities at lower SEP values. The time series of amplitude and phase produced by this model exhibit characteristics consistent with observed data, including the amplitude scintillation index, signal amplitude distributions, and cycle slips during deep fades.

An example PSD spectrum of the amplitude scintillation is presented in Figure 2. Three parts of the spectrum have been identified.

1. A white noise component is observed at frequencies higher than about 10° Hz in the two higher SEP examples (this frequency tends to get higher when the SEP is lower) and corresponds to the thermal noise.
2. A second 'white noise' region where the PSD is flat as a function of frequency that corresponds to the scintillation introduced by the solar corona.
3. A pink noise component at lower frequencies and more noticeable at higher values of SEP (e.g. 5.6° and 9.0°). The PSD level of the pink noise does not appear to systematically depend on SEP, although there is some variation from pass to pass.

The phase, $\phi(t)$ has been described by modeling the PSD of the observed phase variations with a straight line, found by fitting observed data. An example phase PSD is presented in Figure 3. This approach captures the gradual changes in phase introduced by solar plasma effects and helps simulate the cycle slips observed during low-SEP scenarios.

This channel model has been integrated into a comprehensive communication system simulator, which successfully reproduces performance metrics, such as bit error rate

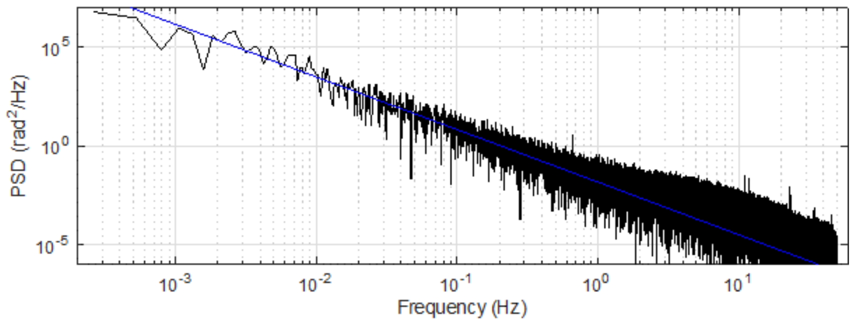

Figure 3. The power spectral density of the phase for an X-band signal on 9 April 2013 for 0737–0840 UT. The straight line is the least-squares fit evaluated between 0.002 and 0.1 Hz (the gradient is -2.66 and the value at 1 Hz is $10^{-1.83}$).

(BER), observed in previous studies (e.g., Kinman, 2003) for various modulation (e.g., binary phase shift keying) and coding techniques (e.g., Turbo coding). This simulation-based approach enabled a detailed assessment of signal stability and performance, providing the basis for the analysis detailed in the following chapters.

3 Coherent Demodulation

Depending on the type of link, bit (and frame) errors can occur due to failure to track changes in the phase or amplitude fading. In this respect, the PLL bandwidth ($2B_L$) is fundamental, since a correct definition can define the threshold between correct or incorrect carrier tracking. For this reason, we introduced a model (here known as an 'analytic' model, although it is a semi-empirical model) for the phase variance that will allow the PLL parameters required for optimum performance to be determined.

3.1 PLL Bandwidth Optimum

The total variance, σ_ϕ^2 is the sum of the phase variance due to the solar coronal scintillation, σ_S^2 and that due to thermal noise, σ_N^2 (Lanucara, 2013). The thermal noise in the PLL is simply proportional to the two-sided PLL bandwidth, $2B_L$, and inversely proportional to the signal-to-noise density, S/N0 *. But the solar variance is a more complicated function of the SEP angle in degrees and $2B_L$ in Hz. This can be expressed as:

$$\sigma_\phi^2 = \frac{C_{band} C_{pll} C_q}{\beta^q (2B_L)^r} + \frac{2B_L}{2CN0_{PLL}} \tag{1}$$

Equation 1 follows the basic form of the JPL model in (Feria et al., 1997), but with different exponents. In our case, β is simply the SEP angle in degrees for X-band, but a function of β for S- and Ka-band; C_{band} depends on whether S, X, or Ka-band is used and on whether the link is an uplink, downlink or an up and down link; C_{pll} depends on whether the PLL used is critically damped or underdamped and C_q depends on the signal quality. The signal quality may be chosen to be 'good', 'moderate', or 'poor' and will determine whether the values in the model are derived from the lower decile, median or upper decile of the scintillation distribution in the data. Furthermore, the exponents, q, and r as well as C_{band}, C_{pll} and C_q take on different values for $\beta < 4.7$ and $\beta > 4.7$.

* Depending on the modulation index we will have a portion of the power provided to the carrier, i.e. C/N0 and a portion to the data, i.e. D/N0.

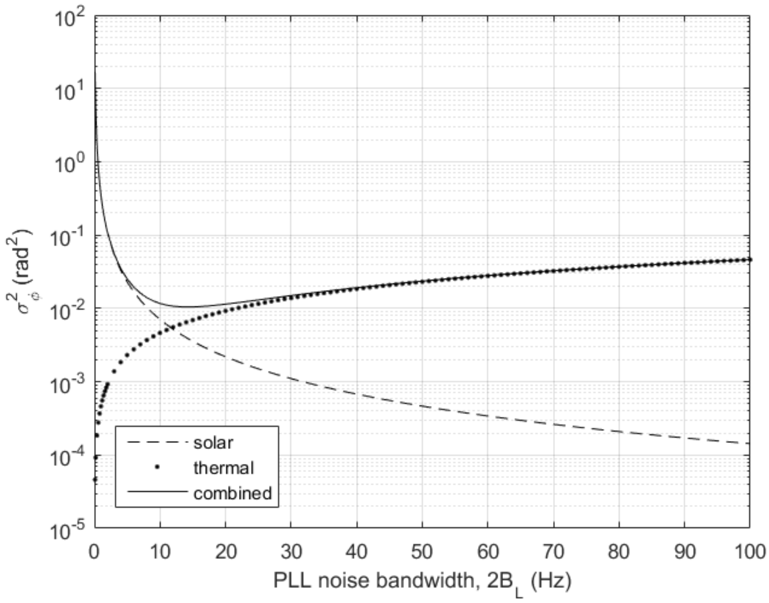

Figure 4. Phase noise vs PLL Bandwidth (2BL) derived from the analytical model for the Jupiter TC Scenario (see Section 4).

Differentiating (1) with respect to the PLL bandwidth and equating it to zero gives the following expression for the optimum value of $2B_L$ (i.e. the value that gives the minimum σ^2_ϕ):

$$(2B_L)_{opt} = [\frac{2SN0_{PLL}C_{band}C_{pll}C_q r}{\beta^q}]^{\frac{1}{r+1}} \tag{2}$$

The PLL bandwidth, 2BL, should be chosen such that it is (Figure 4):

1. large enough to minimize the phase variance caused by the solar plasma;
2. small enough to minimize the thermal noise contribution from the PLL;
3. small enough to maintain an adequate SNR such that the effect of thermal phase jumps is minimized (SNR>10 dB). If there is insufficient carrier power to obtain the required SNR, then increasing 2BL (at the expense of a further reduction in SNR) or decreasing the sample rate will minimize the effect of the phase jumps.

3.2 Fading Model

For SEP values where the amplitude fading is relatively small (e.g. for X-band, at SEP=3°, the fading depth is ∼3 dB), we neglected its effect. For lower SEP, instead, a Nakagami distribution was used to fit the data (A. J. Stocker et al., 2018). The fading model described below determines the phase variance that is exceeded p% of the time, based on the amplitude probability density distributions from thirty-two observed Mars Express 2013 data files. Each file was fitted to a Nakagami distribution, which is defined for positive values of x (here representing the received signal amplitude) using parameters $\mu(> 1/2)$ and $\omega(> 0)$ by:

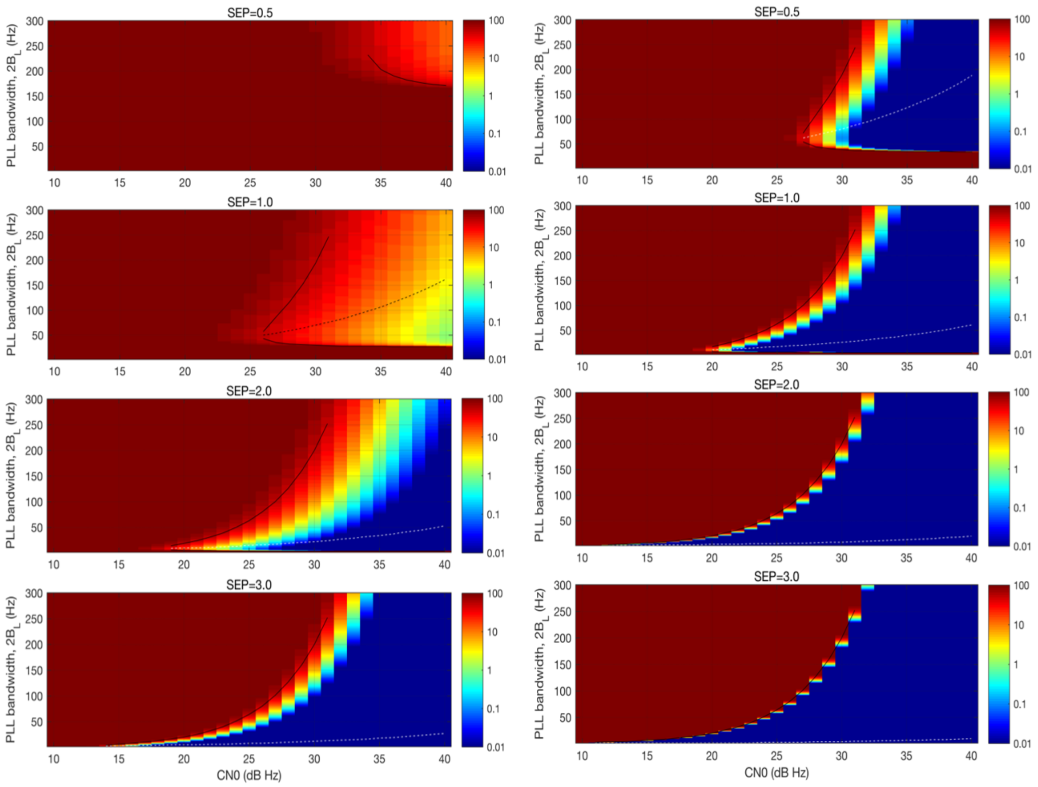

Figure 5. Pcritical (%) (i.e. where phase variance >0.1° rad^2) as a function of PLL bandwidth and CN0 for an X-band (left column) and Ka-Band (right column) downlink at different SEP angles. The solid black lines represent the minimum and maximum values of 2BL for which the total phase variance is <0.1 rad^2 (neglecting fading), while the dashed line (either black or white for clarity) represents the optimum 2BL (i.e. where the phase variance is minimized, neglecting fading)

.

$$N(x, \mu, \omega) = \frac{2\mu^{\mu} x^{(2\mu-1)}}{\omega\Gamma(\mu)} exp(\frac{-\mu x^2}{\omega}) \tag{3}$$

Once ω and μ have been parametrised, a distribution of amplitude for any SEP angle and any percentile can be found from these parameters. For low SEP, the Nakagami distribution was a better fit to the observations than the Rician distribution often employed.

The probability, $P_{critical}$, that the PLL will have difficulty in tracking the phase is presented in Figure 5, where we can see the effect of different values of CN0 and 2BL.

An examination of the figure reveals a number of points:

1. At low SEP, there is a relatively sharp ('cliff edge') value of PLL BW below which the $P_{critical}$ is close or equal to 100% (e.g. for X-band, at SEP=1°, this occurs at about 30 Hz). The PLL bandwidth at which this occurs decreases slowly with increasing CN0 and is higher for smaller SEP.
2. For a given SEP, the value of 2BL that minimizes $P_{critical}$ is essentially constant with changing CN0 (this is at the 'apex' of the color contours, e.g. for X-band,

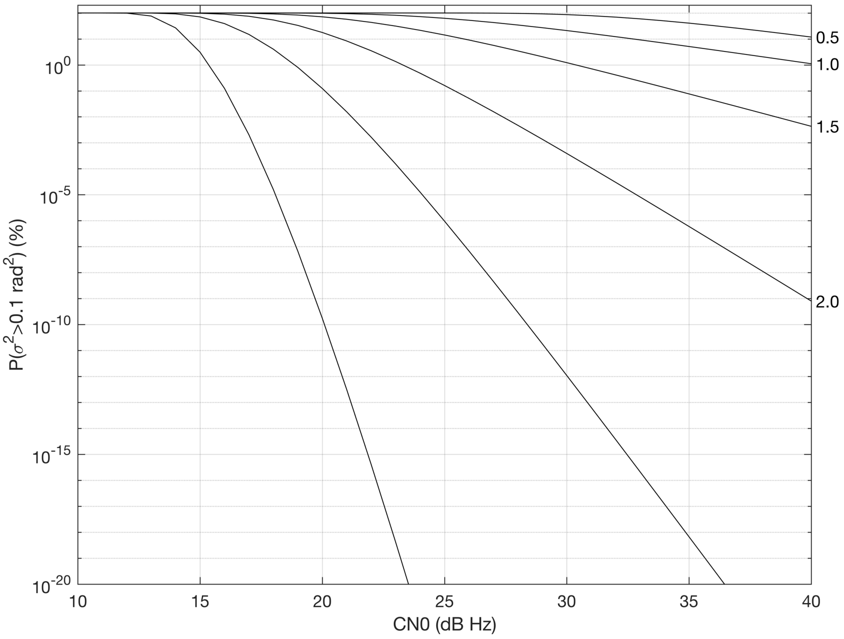

Figure 6. The minimum $P_{critical}$ (so the curves for different SEP are for different 2BL) of an X-band downlink as a function of CN0 for different values of SEP (marked, in degrees, on the right-hand side, the unmarked curves crossing the x-axis at just over 35 dB Hz and just under 25 dB Hz are for SEP of 2.5° and 3.0°, respectively).

.

at SEP=1°, this is approximately 50 Hz). This value of 2BL where the minimum occurs is fairly close to the 'cliff edge' in probability. Given that small changes in the solar plasma will move the cliff edge to different values of 2BL (e.g. if solar conditions were more closely aligned to those 0.5° below the actual SEP then it would be located at higher 2BL and vice versa) it would be unwise to operate the PLL at this bandwidth since it would then result in a high value of $P_{critical}$. It is clear that the value of 2BL that minimizes the $P_{critical}$ is different to that which minimizes the phase variance in the absence of fading (the dashed line) but that the difference between them is greater for smaller SEP (where the fading effects are large) compared to higher SEP (where the fading effects are smaller).

3. For X-band with SEP $\geq 1°$, the minimum value of $P_{critical}$ never falls below 10% at the range of CN0 plotted (increasing the CN0 would reduce this a bit). This can be seen more clearly in Figure 6 which shows the minimum value of $P_{critical}$ at each CN0 for different values of SEP. The value of CN0 required to make the PLL likely to operate reliably depends on what is considered acceptable. For example, to achieve a value of$P_{critical}$ of below 0.01%, then the CN0 would need to exceed about 27 dB Hz for SEP=2° and about 38 dB Hz for SEP=1.5°.
4. For Ka-band, the boundary between where $P_{critical}$ is high and where it is low is sharper than for X-band because of the reduced amplitude fading encountered at Ka-band.
5. For Ka-band, even at SEP=0.5°, there are values of CN0 and 2BL where $P_{critical}$ is low. However, for SEP=0.5° the model is at the limits of its applicability and therefore, some care would be needed in applying these results.

These results indicate that for X-band, using coherent modulation for $1.5° < SEP < 2°$ would allow the PLL to track the solar-induced phase provided CN0 is high (e.g. at

SEP=1.5°, for CN0=40 dB Hz, $P_{critical}$ is just under 0.01%). However, at SEP<1.5°, even if large CN0 was available, the presence of phase slips caused by the deep fading (the effects of which are not included in the model described here) are likely to cause additional problems. Therefore, the performance analysis for coherent modulation on X-band links has focused on SEP>2°.

The following discussion, assumes that, for a residual carrier, the PLL is operated in the region where the phase variance remains below 0.1 rad^2. When the phase variance exceeds this threshold, it is more likely that the PLL will not successfully track the phase. If only thermal noise is present (i.e. the effect of the solar plasma is small, e.g. when SEP is large) then this condition will occur when the double-sided in-loop SNR is less than approximately 7 dB.

4 Analysis of current communication subsystems architecture and operational methods

Using the models and simulator developed within the HELIOS project, the existing communication subsystem architecture and operational procedures have been thoroughly analyzed to identify critical points. An initial overview of this analysis was presented in (A. Stocker et al., 2018), while a more comprehensive discussion is provided here. The analysis focuses on the complete end-to-end communication link and is based on the modulation and coding schemes in use at the time of the study (2018), specifically BPSK modulation, BCH coding for Telecommand (TC), and Turbo 1/4 coding for Telemetry (TM). The analysis has been undertaken for X-band and at a SEP=3°, neglecting the effects of amplitude fading, since the fading depth is 3 dB for X-band at that particular SEP, and this will have a relatively small effect (e.g. in the limit, the simulated data rates will need to be halved). The analysis process was performed on some contingency scenarios, in order to evaluate the link performances and to show that the use of an optimum PLL Bandwidth value can provide a more reliable link. As an example, a hypothetical scenario at Jupiter is used (see Table 1 for the details). The simulation process consists in examining at first the nominal setup, and then trying to optimize it by choosing the optimum PLL bandwidth for that particular scintillation regime. This operation is done using first an analytical equation (see equation 1) and then verified against the simulator (see Figure 4).

Table 1. Nominal and optimized configuration for Jupiter TC Scenario (SEP = 3°)

Jupiter TC	Nominal configuration	Optimized configuration
S/N0 [dB Hz]	31.15	-
Modulation index (m) [rad]	0.6	-
Coding scheme	BCH	-
$2B_L$ [Hz]	30	12
SNRPLL [dBHz]	19.2	15.6
Bs [sps]	8	16

Once the optimum PLL Bw has been determined, the maximum symbol rate that permits a feasible link, i.e. a FER = 10^{-3} for the TC case and a FER = 10^{-5} for TM can be found. This process is done by decreasing the symbol rate progressively (and so increasing the Eb/N0) until the desired performance level is reached. An example can be seen in Figure 7.

So, it was concluded that the link was surely feasible (and not only for this case but for all the contingency scenarios provided). In addition, the usage of the optimum

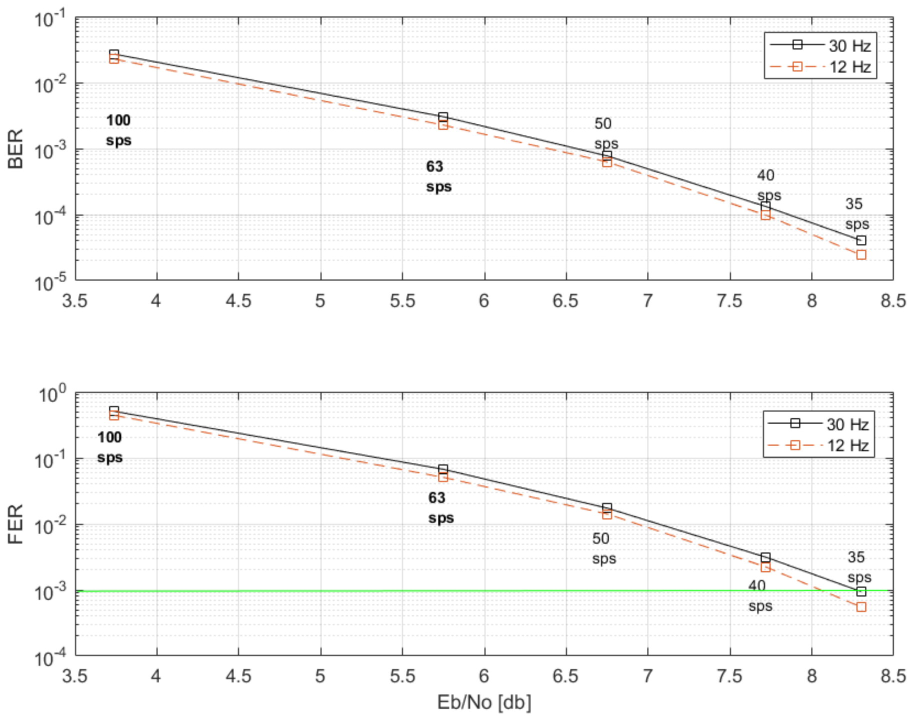

Figure 7. Bit Error Rate (BER) and Frame Error Rate (FER) vs Eb/No for two different PLL Bandwidth (10 and 30 Hz) for the Jupiter TC Scenario.

PLL bandwidth, i.e. the one that minimizes the phase variance, gives the opportunity to improve the performance even more. As said previously, fading was neglected for the simulations of this Section – a straightforward solution, to take it into account, is to add 3 dB (the X-band fading level at SEP=3°) to the required EbN0 to provide fading margin, if this is feasible, or to reduce the data rate by a factor of a half.

5 Proposed and Tested Alternative Solutions

At very low SEP angles, the increased level of amplitude fading means that phase jumps occur and there is an increase, for the duration of a fade, in the thermal phase noise. The two parameters that have a large impact on the PLL performance are its bandwidth and the available CN0. Using different combinations of these two parameters and comparing the phase variance with a threshold value, i.e. 0.1 rad^2, the probability, Pcritical that a PLL would be unlikely to track the phase was obtained (see Figure 6). From this study, it is clear that at X-band, using coherent modulation, with values of the SEP angle lower than 2°, would be problematic unless very high values of CN0 are available (CN0>40 dBHz may be available and this would allow the PLL to operate down to SEP ∼1.5° for X-band). Even if large CN0 were available, the presence of phase slips, caused by the deep amplitude fading are likely to remain a problem. For Ka-band, the intensity of amplitude fading is lower and therefore the PLL tracking is sufficiently robust, thus coherent modulation methods could be used down to SEP$\tilde{1}$° and possibly a little lower than this. For X-Band instead the following solutions were tested.

5.1 New coding schemes

For the TC case, two standardized codes (CCSDS, 2021) were compared: Low-Density Parity Check (LDPC) (64/128 and 256/512) and BCH (57/63). Taking a look at Table 2, it is immediately clear how as the SEP angle decreases, i.e. down to 2° (since this is a SEP angle where the PLL is able to operate with achievable CN0), the two short LDPC codes require a lower Eb/N0 (in dB) compared to the standard BCH (besides having also better performances) to achieve the same FER.

Table 2. Minimum value of Eb/N0 required for the BCH code to reach FER = 10^{-3} at different SEP, and gain (in dB) of the LDPC with respect to the BCH (positive values indicate better performance, i.e. same FER with lower Eb/N0).

SEP (deg)	Standard BCH 57/63	Delta-Eb/N0 for LDPC 64/128	Delta-Eb/N0 for LDPC 256/512
2	9.8 dB	+5.1 dB	+6.2 dB
3	8 dB	+3.6 dB	+4.9 dB
4	7.8 dB	+3.5 dB	+4.7 dB
AWGN	7.65 dB	+3.35 dB	+4.35 dB

Moreover, it is really interesting to note how, if SNR_{PLL} is high enough, such that the phase variance is below a threshold of 0.1 rad^2, which for the AWGN case occurs around 10-7 dB, the performance of the link is not affected by the S/N0 (see Figure 8). Note that, in the case of Figure 8, the PLL Bw used is fixed, so as a consequence is not the optimum for each point. If this would have been the case, the isolines would have been vertical (till the minimum SNR_{PLL} value, i.e. 7 dBHz), meaning that the performances are independent of the S/N0 provided enough power is available for the carrier.

Table 3. minimum value of Eb/N0 [dB] required for the different codes to reach FER = 10^{-5} at different SEP

SEP (deg)	LDPC 1024	LDPC 4096	Turbo 1/2	Turbo 1/4	Turbo 1/6
2	∼2.5 dB	∼1.8 dB	∼1.55 dB	∼0.3 dB	∼-0.05 dB
3	∼2.03 dB	∼1.4 dB	∼1.38 dB	∼0.24 dB	∼-0.1 dB
4	∼2.01 dB	∼1.32 dB	∼1.25 dB	∼0.23 dB	-

For the TM case, LDPC and Turbo codes are compared. By considering the targeted FER performance of the project, i.e 10^{-5}, a few considerations can be made:

1. Turbo code with a code rate of 1/2 (considered here to have a fair comparison with LDPC) has an advantage over the shorter LDPC, i.e. k= 1024, both in terms of the minimum Eb/N0 [dB] and as a consequence also in terms of maximum bit rate (see Table 3). While with respect to the “medium length” LDPC, i.e. k = 4096 the advantage is not so marked.
2. The Turbo code encoder is less complex than that of the LDPC codes.

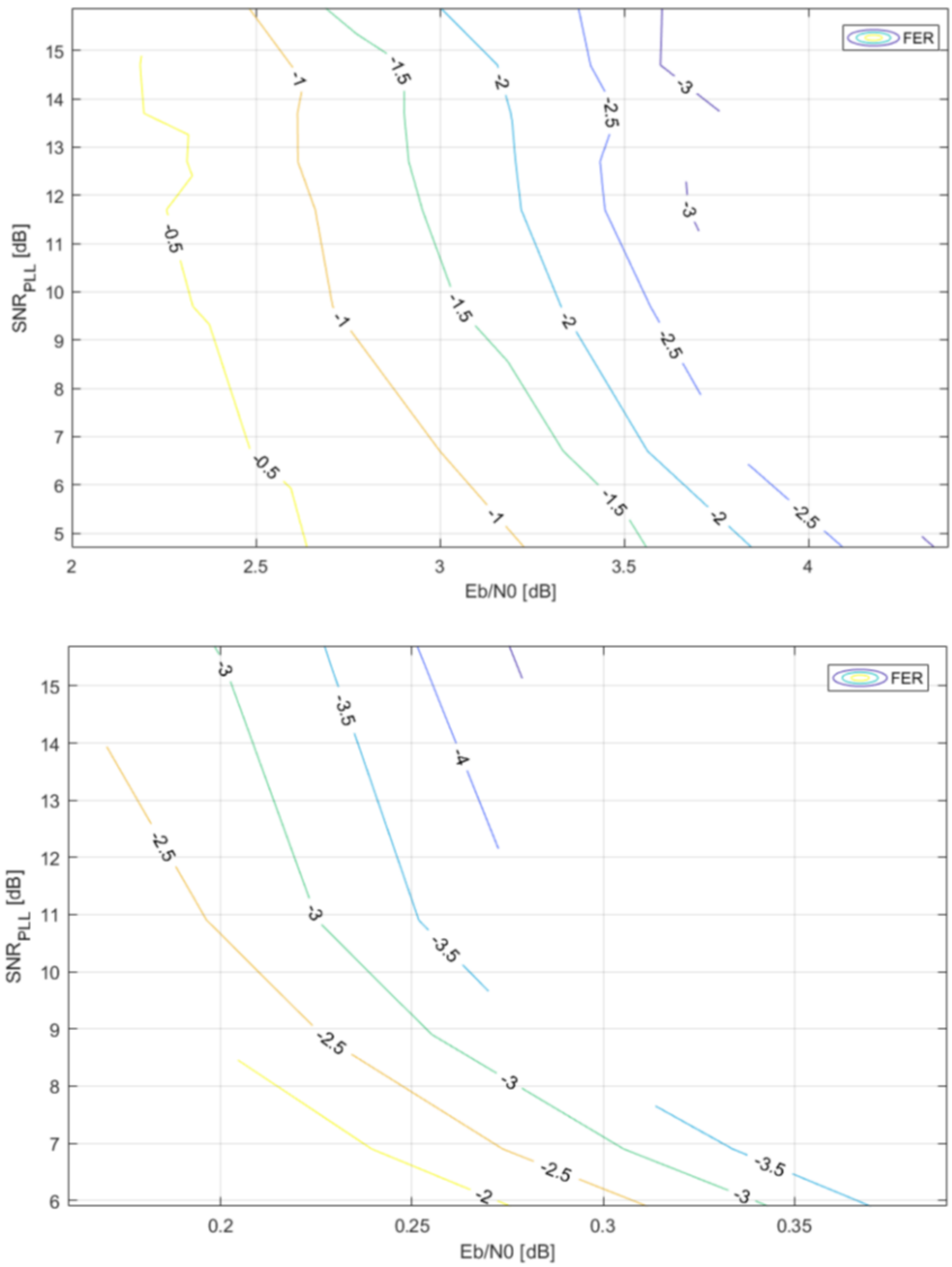

Figure 8. Isolines of FER (Frame Error Rate) for different values of Eb/N0 and SNR_{PLL}. Top picture shows the LDPC 256/512 code with a SEP of 2° and a PLL bandwidth of 28 Hz for a TC scenario, while the bottom figure shows the case of a Turbo 1/4 code, with SEP = 2° and PLL bandwidth of 20 dB for a TM scenario.

3. Above a certain Eb/N0, Turbo code 1/2 shows an "error floor"†, that in the case of SEP =2°,3° happens exactly at the target FER considered.

† even though Eb/N0 increases the values of BER/FER remain almost constant

So, even if the Turbo Code shows slightly better performances and less complexity, probably the LDPC k = 4096 should be the safest choice since even a small change in the solar condition could cause a failure of the Turbo code.

5.2 Ergodicity

In order to draw conclusions about the impact of solar plasma at low SEP values on the performance of CCSDS channel codes for uplink and downlink, it is useful to compare the channel coherence time Tc, i.e. the time duration over which the channel impulse response is considered to be not varying, with the time needed to transmit the generic codeword. The channel coherence time was derived from the X-band observations made during the MEX 2013 solar conjunction. According to that analysis, the channel coherence time values are as follows:

- for SEP = 3° the Tc is 30 ms
- for SEP = 2° the Tc is 18.75 ms
- for SEP = 1° the Tc is 6.35 ms

The knowledge of the channel coherence time Tc is important as it allows the solar plasma channel to be approximated as a (frequency-flat) block-fading channel. The channel may be modeled as non-frequency selective owing to the narrow signal bandwidth arising from the low bit rates. According to the block-fading channel model, the fading (arising, in this case, as a consequence of the solar plasma) remains constant over an interval of time equal to the channel coherence time. At the end of this time interval, the level of fading changes to a new value independent of the previous ones. In each coherence time, the fading realization is drawn according to a channel-specific probability density function. When a channel code of codeword length n is transmitted over a block fading channel, it is common to define the channel diversity as the number of independent fading levels experienced by each codeword. The channel diversity is hereafter denoted by L. If the time required to transmit one channel symbol is (sufficiently) higher than the channel coherence time, then fading may be assumed as independent from symbol to symbol. This situation, in which the fading channel is memoryless, is sometimes referred to as the "ergodic case". The channel diversity in the ergodic case is equal to the codeword length, i.e., L=n. On the other hand, when the channel coherence time spans a number of consecutive channel symbols the block-fading channel is the correct channel model. From the perspective of the generic codeword, the channel remains stationary but is "non-ergodic", as any fading temporal mean performed over one codeword may diverge significantly from the corresponding statistical mean.

Some parametric curves were obtained, where the "ergodic region" is defined for values of L greater than 100, and the "non-ergodic region" for values[‡] less than 10 (see Figure 9).

We have to keep in mind that all these considerations are made for the contingency cases studied, which have a similar S/N0 region of operation. So, in nominal cases, the S/N0 value at our disposal will be higher, this means having larger symbol rate values and so a larger diversity. Coding schemes that in our study are considered "safe", i.e. inside the ergodic-one, could well be in the non-ergodic region in nominal cases. What we provide here are guidelines based on a few contingency cases, but a detailed analysis may be needed on a case by case basis. So, taking into consideration Figure 9, we note that for a D/N0 [§] higher than 35 dB Hz (for SEP = 2°) and 32 dB Hz (SEP = 3°), the channel diversity (L), is lower than 10, so this suggests that in this case any kind of tech-

[‡] These values are valid for a SEP = 3° and 2°, for SEP = 1° the values of L considered are higher

[§] here D/N0 is intended as the portion of S/N0 that is used for the data

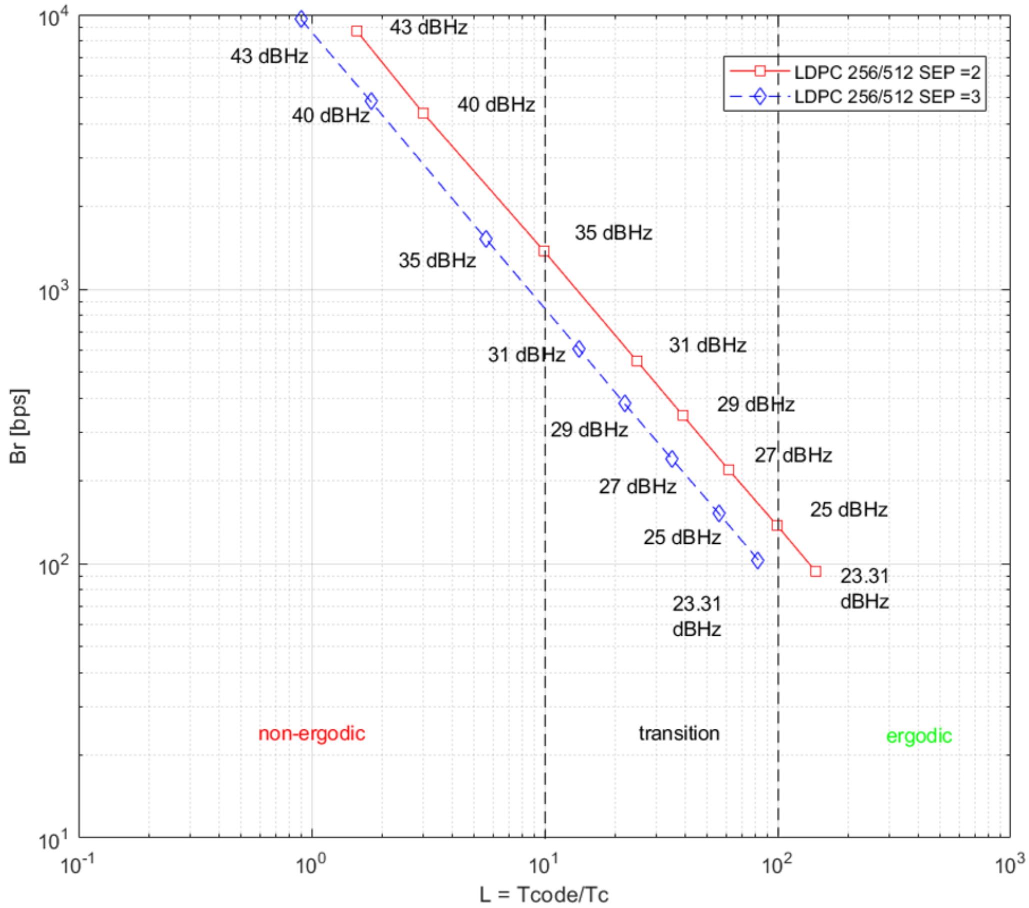

Figure 9. Channel diversity vs bit rate for the BCH 57/63 code at two different SEP angles. Each point in the curves has the indication of the D/N0 [dBHz] corresponding to that case.

nique that can increase L should be effective in increasing the performance of the code, i.e. obtaining a lower FER keeping the other parameters constant. As stated above, a simple way to increase the diversity is by the use of an interleaver. Conversely, when L is higher than 10, even if one could increase it, the attainable gain in terms of BER/FER is negligible (since we are approaching the "ergodic case").

5.3 Non Coherent FSK Modulation

In order to have an idea of the potentiality of non-coherent modulation at low SEP angles, a set of simulations was performed using an MFSK modulation, with different M values, i.e. 2, 4, 8, 16, at first without any coding, and then using an LDPC with different frame length for TC and TM. The results of the uncoded case were compared with those of the LDPC codes in order to see, first of all, if the link was feasible at SEP = 1° for our contingency cases of interest and then also to see how the LDPC codes, that are in principle not designed for this kind of modulation, perform.

Obviously, the performances could be improved, since the LDPC coding schemes have been specifically designed and optimized assuming different coherent modulations (BPSK and QPSK) and the AWGN channel. There is, in principle, no reason why these coding schemes should perform close to the theoretical limits also with nonlinear mod-

Table 4. Values of Eb/N0 [dB] for which the target FER, i.e. 10^{-5} is reached at SEP = 1 ° for the Uncoded (fixed Br = 300 bps) and LDPC k=256 non-coherent M-FSK modulation at an S/N0 = 28 dBHz and the respective gains compared to the non-coherent 2-FSK

modulation	UNC Eb/N0 FER	Gain wrt 2-FSK	LDPC Eb/N0 FER	Gain wrt 2-FSK
2-FSK	38 dB	- dB	13.6 dB	- dB
4-FSK	35 dB	3 dB	12.3 dB	1.3 dB
8-FSK	33.6 dB	4.4 dB	11.8 dB	1.8 dB
16-FSK	32.7 dB	5.3 dB	11.7 dB	1.9 dB

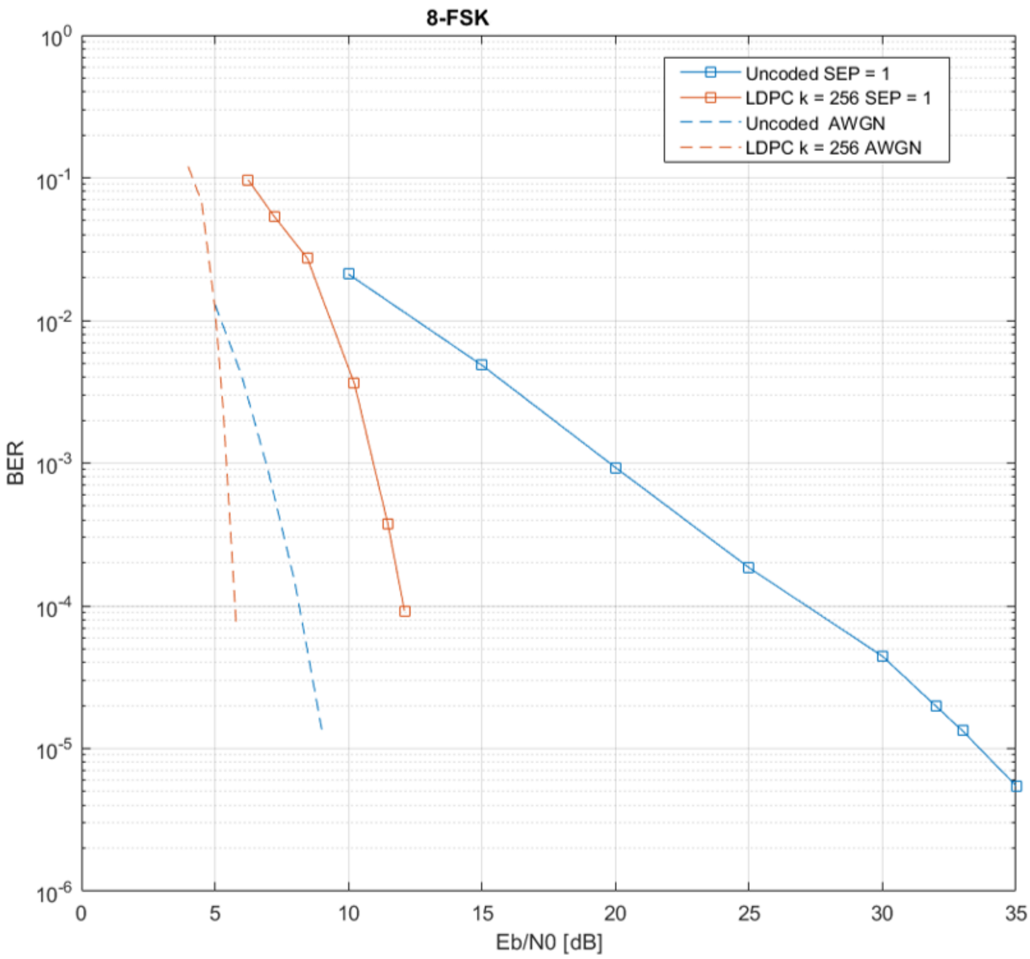

Figure 10. BER (Bit Error Rate) vs Eb/N0 [dB] for non-coherent 8-FSK modulation with an LDPC k = 256 and Uncoded case, at SEP = 1° and AWGN.

ulations (such as M-FSK) and over channels with a nonergodic behavior. But still, the LDPC codes are better (in terms of final performances) than uncoded. At very low SEP angles in particular, the degradation seen in the uncoded case is significantly larger than the one seen on LDPC (see Figure 10).

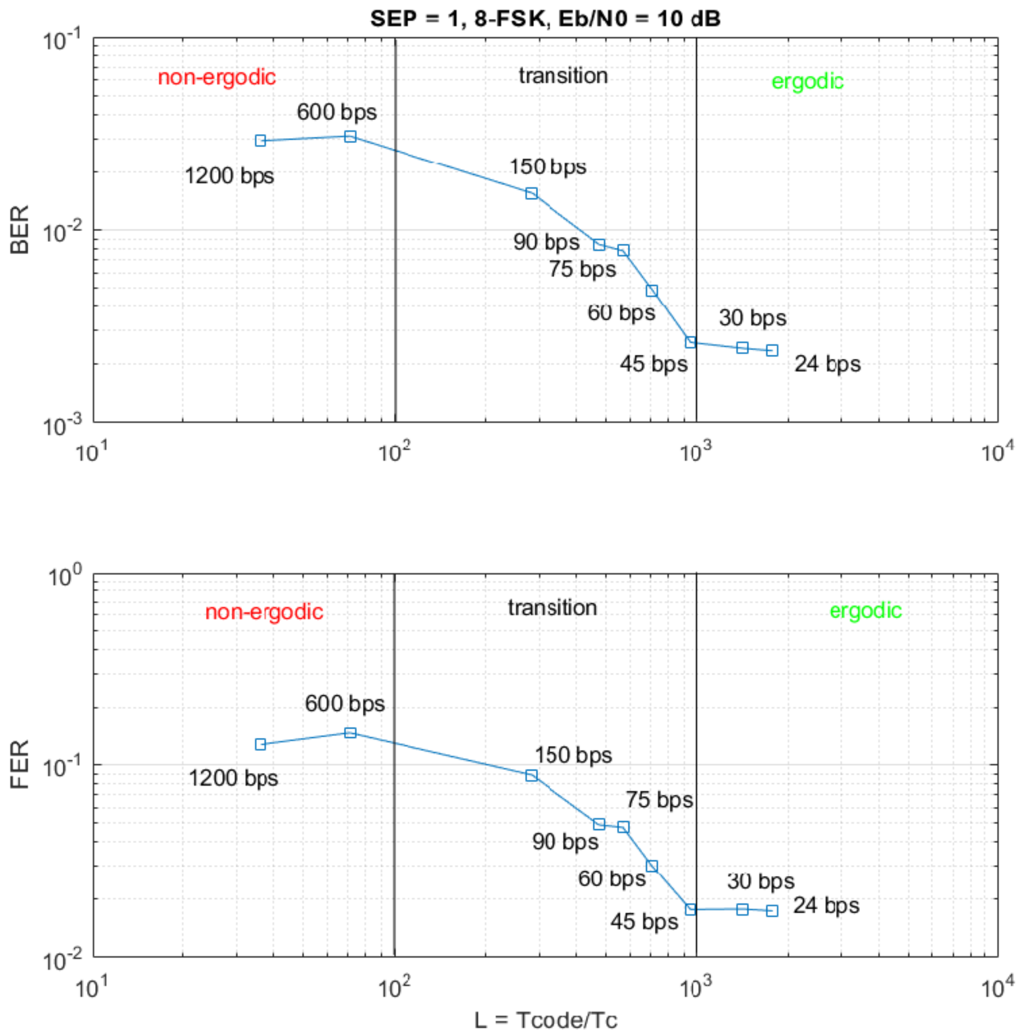

Figure 11. Channel diversity vs bit rate for the LDPC k=256 code at a SEP angle of 1° and a non-coherent 8-FSK modulation. Each point in the curves has the indication of the S/N0 [dBHz] corresponding to that case.

An ad-hoc code design may lead to new codes achieving higher coding gains. Moreover, the channel diversity plays a fundamental role, since as soon as we approach the "non-ergodic zone", the performances tend to degrade very quickly (see Figure 11), so most probably, any technique that can increase the channel diversity value (like interleaving) will bring a huge improvement in the performances.

6 Conclusions

Different solutions have been proposed to improve the reliability of RF TT&C links during Superior Solar Conjunctions. In particular, when the SEP angle is higher than 2°, for X-Band links, the Phase Locked Loop (PLL) is still able to lock and track the signal, so, an appropriate tuning of its parameters (mostly the bandwidth) can improve the quality of the link and allow us to reach higher symbol rates at the same available power level. Another viable approach consists in the use of alternative coding schemes, i.e. Low

Parity Denisty Check (LDPC), which shows promising results, especially in sending TC, where the required Eb/N0 to achieve the same value of FER is 5-6 dB lower for the LDPC 256/512 than for BCH. In the case of reception of TM data, although Turbo code has slightly better performance than LDPC, the use of the latter is still suggested since it is more robust to sudden changes in the solar conditions at the targeted FER. When the SEP angle is around 1.5° or below, standard coherent modulation is no longer effective, so new techniques are required. One involves the use of non-coherent modulation, like Frequency Shift Keying (FSK), which has proven to be very robust to solar plasma at very low SEP angles, outperforming standard BPSK. The simulations performed during the study show that a feasible link at SEP = 1° is possible using FSK and also that the use of coding schemes, like LDPC, can help increase the performance even further. All of this taking into consideration that the coding schemes used for the study are not optimized for this specific case (they were developed having in mind a coherent modulator/demodulator), so they are not optimal. The other proposed solution involves the use of techniques that are able to increase the channel diversity (L) and, as a consequence, make the code more robust to deep fading events. In cases where the channel diversity is lower than a certain threshold, we are in a "non-ergodic" case, and any technique that is able to increase L (like interleaving for example), should be effective in improving the performance of the code too. The simulations performed show that there are several cases, among the ones studied, that can benefit from these techniques.

Acknowledgments

The work described here was carried out under a contract with the European Space Agency (Contract No. 4000112986/14/F/MOS - HELIOS - Highly rEliable LInks during sOlar conjunctionS) funded by the General Study Programme (GSP) under Invitation to Tender AO/1-8050/14/F/MOS.

References

Armstrong, J. W., Woo, R., & Estabrook, F. B. (1979). Interplanetary phase scintillation and the search for very low frequency gravitational radiation. , *230*, 570. Retrieved 2024-09-24, from http://adsabs.harvard.edu/doi/10.1086/157114 doi: 10.1086/157114

Bertotti, B., Comoretto, G., & Iess, L. (1993). Doppler tracking of spacecraft with multi-frequency links. , *269*, 608–616. Retrieved from https://api.semanticscholar.org/CorpusID:109810456

CCSDS. (2021). *TC synchronization and channel coding* (No. CCSDS 231.0-B-4). CCSDS Secretariat National Aeronautics and Space Administration.

Feria, Y., Belongie, M., McPheeters, T., & Tan, H. (1997). Solar scintillation effects on telecommunication links at ka-band and x-band. , *129*, 1–11. Retrieved 2023-08-06, from https://ui.adsabs.harvard.edu/abs/1997TDAPR.129A...1F (ADS Bibcode: 1997TDAPR.129A...1F)

Finocchiaro, S., Ardito, A., Barbaglio, F., Baldi, M., Chiaraluce, F., Maturo, N., ... Mercolino, M. (2017). Improving deep space telecommunications during solar superior conjunctions. In *2017 IEEE aerospace conference* (pp. 1–13). IEEE. Retrieved 2024-10-31, from http://ieeexplore.ieee.org/document/7943738/ doi: 10.1109/AERO.2017.7943738

Ho, C. (2005). *106, rev. b - solar corona and solar wind effects.* DSMS Telecommunications Link Design Handbook.

Kinman, P. (2003). 207, rev. a 34-m and 70-m telemetry reception. In *DSMS telecommunications link design handbook.*

Lanucara, M. (2013). *Spacelink impairments by solar effects.* ESA Document, Issue 2, Rev. 0.

Li, Q., Yin, L., & Lu, J. (2012). Performance study of a deep space communications system with low-density parity-check coding under solar scintillation.. Retrieved from https://api.semanticscholar.org/CorpusID:85555606

Mariotti, G., & Tortora, P. (2013). Experimental validation of a dual uplink multi-frequency dispersive noise calibration scheme for deep space tracking. , *48*(2), 111–117. Retrieved 2025-02-04, from https://agupubs.onlinelibrary.wiley.com/doi/10.1002/rds.20024 doi: 10.1002/rds.20024

Morabito, D., Shambayati, S., Finley, S., & Fort, D. (2003). The cassini may 2000 solar conjunction. , *51*(2), 201–219. Retrieved 2023-05-04, from http://ieeexplore.ieee.org/document/1195647/ doi: 10.1109/TAP.2003.809055

Morabito, D. D. (2007). Solar corona-induced fluctuations on spacecraft signal amplitude observed during solar superior conjunctions of the cassini spacecraft: SOLAR CORONA-INDUCED FLUCTUATIONS. , *42*(3), n/a–n/a. Retrieved 2023-05-04, from http://doi.wiley.com/10.1029/2005RS003425 doi: 10.1029/2005RS003425

Pätzold, M., Hahn, M., Tellmann, S., Häusler, B., Bird, M. K., Tyler, G. L., … Tsurutani, B. T. (2012). Coronal density structures and CMEs: Superior solar conjunctions of mars express, venus express, and rosetta: 2004, 2006, and 2008. , *279*(1), 127–152. Retrieved 2024-10-05, from http://link.springer.com/10.1007/s11207-012-9991-y doi: 10.1007/s11207-012-9991-y

Stocker, A., Argyriou, A., Giorgetti, A., Paolini, E., Siddle, D., Tortora, P., … Mercolino, M. (2018). Simulating the reliability of radio links during superior solar conjunctions. In *12th european conference on antennas and propagation (EuCAP 2018)* (pp. 902 (5 pp.)–902 (5 pp.)). Institution of Engineering and Technology. Retrieved 2023-04-28, from https://digital-library.theiet.org/content/conferences/10.1049/cp.2018.1261 doi: 10.1049/cp.2018.1261

Stocker, A., Siddle, D., Warrington, E., Mariotti, G., Silvestri, D., Zeqai, A., … Mercolino, M. (2017). A channel model for the propagation of x-band radio waves through the solar corona. In *Loughborough antennas & propagation conference (LAPC 2017).* Institution of Engineering and Technology. Retrieved 2025-04-21, from https://digital-library.theiet.org/content/conferences/10.1049/cp.2017.0306 doi: 10.1049/cp.2017.0306

Stocker, A. J., Siddle, D. R., Warrington, E. M., Mariotti, G., Silvestri, D., Zeqaj, A., … Mercolino, M. (2018). An x band radio channel model for propagation through the solar corona. , *53*(9), 1014–1022. Retrieved 2023-04-28, from http://doi.wiley.com/10.1029/2018RS006578 doi: 10.1029/2018RS006578

Tortora, P., Iess, L., & Ekelund, J. E. (2002). *Accurate navigation of deep space probes using multifrequency links: the cassini breakthrough during solar conjunction experiments.* Retrieved 2024-09-24, from https://ui.adsabs.harvard.edu/abs/2002iaf..confE.675T (Conference Name: IAF abstracts, 34th COSPAR Scientific Assembly Pages: 675 ADS Bibcode: 2002iaf..confE.675T)

Verma, A. K., Fienga, A., Laskar, J., Issautier, K., Manche, H., & Gastineau, M. (2013). Electron density distribution and solar plasma correction of radio signals using MGS, MEX, and VEX spacecraft navigation data and its application to planetary ephemerides. , *550*, A124. Retrieved 2023-05-04, from http://www.aanda.org/10.1051/0004-6361/201219883 doi: 10.1051/0004-6361/201219883

Woo, R., & Armstrong, J. W. (1979). Spacecraft radio scattering observations of the power spectrum of electron density fluctuations in the solar wind. , *84*, 7288. Retrieved 2023-05-04, from http://doi.wiley.com/10.1029/JA084iA12p07288 doi: 10.1029/JA084iA12p07288

Woo, R., Yang, F.-C., & Ishimaru, A. (1976). Structure of density fluctuations near the sun deduced from pioneer-6 spectral broadening measurements. , *210*, 593. Retrieved 2023-05-04, from http://adsabs.harvard.edu/doi/10.1086/

154864 doi: 10.1086/154864

Woo, R., Yang, F.-C., Yip, K. W., & Kendall, W. B. (1976). Measurements of large-scale density fluctuations in the solar wind using dual-frequency phase scintillations. , *210*, 568. Retrieved 2023-05-04, from http://adsabs.harvard.edu/doi/10.1086/154861 doi: 10.1086/154861